INTERNATIONAL JOURNAL FOR NUMERICAL METHODS IN FLUIDS
Int. J. Numer. Meth. Fluids **28**: 1013–1031 (1998)

THE AGE METHOD FOR DIRECT NUMERICAL SIMULATION OF TURBULENT SHEAR FLOW

DAVID K. BISSET*

Department of Mechanical Engineering, The University of Newcastle, Callaghan, NSW 2308, Australia

SUMMARY

The advected grid explicit (AGE) method for direct numerical simulation of 'incompressible' turbulent shear flows is presented. The Navier–Stokes equations are used for momentum in a velocity–pressure formulation. Mass continuity and an equation of state link pressure with density (which is not assumed identically constant). Time advancement is entirely explicit, and spatial representation is localized (e.g. finite difference) and centred. Magnitudes of non-linear terms are reduced on advected grid(s), and numerical instabilities are efficiently reduced by 'targeted diffusion'. Computation time scales directly on the number of grid points (virtual memory issues aside), and is very short for a DNS method. A spatially developing two-stream mixing layer was simulated as an example, reaching a vorticity thickness Reynolds number $> 20\,000$. Comparison with experimental results from self-similar mixing layers is satisfactory in terms of growth rate and Reynolds stress profiles. Turbulent vortical structures are visualized by means of pressure surfaces. © 1998 John Wiley & Sons, Ltd.

KEY WORDS: advected grid; mixing layer; spatial development

1. INTRODUCTION

It is widely accepted that the Navier–Stokes (NS) equations provide a very good model of the flow of Newtonian fluids, and that numerical or analytical solutions to the equations with appropriate boundary conditions describe real flows very successfully. If the flow is turbulent, the solution is likely to be numerical rather than analytical, but the NS equations still apply as long as the fluid can be treated as a continuum.

Numerical solutions to the full NS equations are relatively rare under the conditions considered here, namely, simple turbulent shear flows of 'incompressible' fluid at moderate Reynolds number (and low subsonic Mach number). Most commercial applications and many research applications of computational fluid dynamics (CFD) do not attempt to solve the NS equations, but instead solve a modified set of equations, e.g. the Reynolds-averaged NS equations with one of many closure schemes, or the NS equations in only two dimensions. The field of large eddy simulation (LES) is also very active [1]. Several comprehensive monographs are available that review all the approaches, e.g. Roach [2], Peyret and Taylor [3], the two volumes by Fletcher [4], and Ferziger and Peric [5], and there are too many specialised review articles to list.

* Correspondence to: Department of Mechanical Engineering, The University of Newcastle, Callaghan, NSW 2308, Australia. Fax: + 61 2 49216946; E-mail: medkb@cc.newcastle.edu.au

CCC 0271–2091/98/171013–19$17.50

Received 14 April 1997
Revised 8 December 1997

Spectral or pseudospectral methods seem to be regarded as the most efficient and accurate methods for full NS solutions (see e.g. Reference [6] for a description). Successful spectral simulations of fully-developed turbulent flows include the channel flows of Moin and co-workers [7–9], the turbulent boundary layer of Spalart [10], and the temporal two-stream mixing layer of Rogers and Moser [11,12]. Very large amounts of CPU time and memory on the largest computers of the day were required, e.g. hundreds of hours were needed for some of the runs in Reference [12]. Other methods are sometimes used, e.g. Rai and Moin [13] used a high-order finite difference scheme of similar computational efficiency for channel flow. There are also some significant spectral method papers, e.g. the temporal two-stream mixing layers of Metcalfe *et al.* [14] and Comte *et al.* [15], in which the flow does not reach a fully-developed turbulent state, at least partly because of computer resource limitations.

In any direct numerical simulation, the calculation domain must carry a lot of detail because of the wide range of scales in turbulence, and the time steps must be small and numerous for the same reason, so a large computational effort will be needed. However, spectral methods and methods with implicit time stepping couple together all parts of the domain at every time step, which requires enormous computational effort, and the effort needed for significant increases in Reynolds number is prohibitive. From a physical point of view this high degree of full-domain interaction does not seem to be necessary, given that the short term development of turbulent motion at one end of the domain is independent of that at the other end. Therefore, the author investigated computationally cheaper methods of calculation where flow development depends mainly on local interactions, including fully explicit advancement in time and finite differences or certain finite volume approaches for spatial discretization. Possible truncation of the range of viscous scales directly simulated (a kind of implied LES) will be discussed later.

Apparently there is very little current work on full simulation methods for turbulent flows of the present type with purely explicit time stepping. One reason, from the present author's initial attempts, is that the non-linear terms in the NS equations cause serious stability problems. This paper will explain how the advected grid explicit (AGE) method achieves stability, and will provide an example of its application to a simple turbulent free shear flow, i.e. a two-stream mixing layer. Work underway on wall-bounded flows will be reported later. The method has been developed for 'incompressible' flows, but it could most likely be applied to subsonic compressible flows also.

Aims in the ongoing development of the AGE method include

(a) computational effort will be small enough for worthwhile results to be produced on readily available computers;
(b) all significant aspects of turbulent flow will be realistically portrayed (though 'significant aspects' is a function of the reasons for doing a simulation); and
(c) responses to changes in boundary conditions will be realistic qualitatively and, if possible, quantitatively.

Solutions will be time-dependent and three-dimensional, although in many cases the solution will be statistically stationary in time and in one or more spatial directions. The AGE method is intended not as a direct competitor for pseudospectral methods, but as an alternative in which greater versatility and speed can be achieved at (possibly) some cost in accuracy.

2. THE AGE METHOD

2.1. Formulation

It is normal, in other methods for 'incompressible' non-stratified flows as considered here, to eliminate certain terms from the NS and mass continuity equations by ignoring gravitational effects and by assuming that both density ρ and dynamic viscosity μ are constant. The usual practice is followed here for gravity and viscosity, but it is assumed that although density variations are small enough to be ignored within the NS equations and within the transport terms ($U\,\partial\rho/\partial x$, etc.) of the mass continuity equation, density is not a constant. There are two reasons for this.

Firstly, truly constant density implies that the entire velocity field must be completely consistent at all times. This is not a problem for analytical solutions, but numerical solutions inevitably contain small errors which imply changes in density and hence contradict the initial assumption. The result could be singularities and numerical instability. Computationally expensive methods such as spectral methods, or very high-order finite difference methods with upwind biased derivatives [13], must be used to achieve sufficient accuracy and stability.

Secondly, density variations provide a means for calculating the pressure field. Local pressure gradients are very important for turbulent flow: they are responsible for the centripetal acceleration essential to the predominant swirling, vortex-like motions of turbulence, which means that there may be advantages in expressing pressure directly. Methods that assume strict incompressibility often eliminate the calculation of pressure by using e.g. a Poisson type variable [13] or a vorticity formulation [11,12]; see also Reference [4] (Section 17.4) or Reference [5] (Ch. 7). In fact Ferziger and Peric [5] state in a rather general context (pp. 159) that the present formulation 'is not appropriate for incompressible or low Mach number flows', but perhaps this statement does not account for the particular properties of turbulent flow.

The NS equations become

$$\begin{aligned}
\frac{\partial U}{\partial t} &= -\left(U\frac{\partial U}{\partial x}+V\frac{\partial U}{\partial y}+W\frac{\partial U}{\partial z}+\frac{1}{\rho}\frac{\partial P}{\partial x}\right)+\nu\left(\frac{\partial^2 U}{\partial x^2}+\frac{\partial^2 U}{\partial y^2}+\frac{\partial^2 U}{\partial z^2}\right),\\
\frac{\partial V}{\partial t} &= -\left(U\frac{\partial V}{\partial x}+V\frac{\partial V}{\partial y}+W\frac{\partial V}{\partial z}+\frac{1}{\rho}\frac{\partial P}{\partial y}\right)+\nu\left(\frac{\partial^2 V}{\partial x^2}+\frac{\partial^2 V}{\partial y^2}+\frac{\partial^2 V}{\partial z^2}\right),\\
\frac{\partial W}{\partial t} &= -\left(U\frac{\partial W}{\partial x}+V\frac{\partial W}{\partial y}+W\frac{\partial W}{\partial z}+\frac{1}{\rho}\frac{\partial P}{\partial z}\right)+\nu\left(\frac{\partial^2 W}{\partial x^2}+\frac{\partial^2 W}{\partial y^2}+\frac{\partial^2 W}{\partial z^2}\right),
\end{aligned} \tag{1}$$

and the mass continuity equation becomes

$$\frac{\partial \rho}{\partial t} = -\rho\left(\frac{\partial U}{\partial x}+\frac{\partial V}{\partial y}+\frac{\partial W}{\partial z}\right), \tag{2}$$

where U, V and W are the longitudinal, transverse and spanwise components of velocity, P is pressure, t is time and $\nu\ (=\mu/\rho)$ is kinematic viscosity. (Local means $\bar{U}(x,y)$ and fluctuations u are also defined, i.e. $U=\bar{U}+u$, etc.) The isentropic relationship between pressure and density for an ideal gas is

$$\frac{\mathrm{d}P}{\mathrm{d}\rho} = k\frac{P}{\rho} = c^2, \tag{3}$$

where k is the specific heat ratio and c is the speed of sound; or for a liquid

$$\frac{\mathrm{d}P}{\mathrm{d}\rho} = \frac{E_v}{\rho} = c^2, \tag{4}$$

where E_v is the bulk modulus of elasticity. The right-hand-side of Equation (3) is of the order 10^5 in SI units for atmospheric air, and that of Equation (4) is $> 10^6$ for water, so it can be seen by writing

$$\frac{\partial P}{\partial t} = \frac{\partial P}{\partial \rho}\frac{\partial \rho}{\partial t} = -c^2\rho\left(\frac{\partial U}{\partial x} + \frac{\partial V}{\partial y} + \frac{\partial W}{\partial z}\right), \tag{5}$$

that the rather small values of $\partial\rho/\partial t$ to be expected from Equation (2) can nevertheless give rise to significant values of $\partial P/\partial t$.

Equations (1) and (5), with specified boundary conditions, are the fundamental equations used by the AGE method. Sound waves are transmitted through the fluid with this formulation, which can be a nuisance at the boundaries.

A very similar formulation in the 'method of artificial compressibility' was used by Chorin [16] for improving the convergence of steady state solutions, and foreshadowed for time-dependent problems. That method uses Equation (2) and substitutes the variable density for pressure in Equation (1) via an artificial equation of state. However, the aim was to provide a means of iteration that would approach true incompressibility. Peyret and Taylor [3] (Ch. 6) and Fletcher [4] (Ch. 17) discuss the method and give further references. In the AGE method, pressure and (small) density gradients are treated as real, not artificial, but there is still a measure of empiricism in the numerical implementation.

It is also interesting to consider the discussion by Hirt and Harlow [17] of general corrective procedures that reduce the number of iterations for iterative methods. Effectively the inconsistencies remaining when iteration is not fully converged are carried forward into the next time step as a correction term. In the AGE method the pressure variations calculated from Equation (5) include automatic compensation for errors in previous calculations of velocities. The compensating pressure values are carried forward into the next velocity calculation (iteration is not required because there is no assumption of strict incompressibility).

2.2. Numerical approach

2.2.1. General procedure. Variables U, V, W and P are defined at two time levels on the vertices of an IJK grid. Standard SI units are used. The grid plane spacings are Δx (constant), Δy (varies in y) and Δz (varies in z). Variable spacing is not really needed for the mixing layer simulation given below, but was implemented with an eye towards wall-bounded flows in future. In Equation (1) P is stored as a deviation from a global mean to improve resolution when calculating differences, and $c^2\rho$ is taken as a constant in Equation (5). Central differences are used for spatial derivatives, and time stepping is first-order explicit (hence the requirement to store variables in two alternating sets of arrays representing two time levels). The size of the time step Δt appears to be limited by the time taken for a pressure wave travelling at speed c to traverse the smallest grid plane separation.

The general procedure for time advancement is to use current velocities and pressures to calculate new pressures via Equation (5), and then to calculate new velocities via Equation (1). The calculated pressures could be regarded as falling halfway in time between old and new velocities, and therefore a predictor–corrector approach for the velocity calculations could be tried. Also, the spatial derivatives are second-order at present, but fourth-order spatial

derivatives would be straightforward to implement. Nevertheless, it is significant that the method works in its present simple form. Note that there are no procedures that would prevent efficient use of vector or parallel computers.

2.2.2. Pressure calculation. New pressures are actually calculated from a modified Equation (5), i.e.

$$p^{n+1} = p^n_{\mathrm{sm}} - \Delta t\, c^2 \rho \left(\frac{\partial U}{\partial x} + \frac{\partial V}{\partial y} + \frac{\partial W}{\partial z} \right)^n,$$

where $n+1$ and n indicate new and current times, and

$$p^n_{\mathrm{sm}} = (W_p) p^n + (1 - W_p) \sum (\text{six neighbouring pressures})/6,$$

where W_p is a constant between 0.0 and 1.0 that acts as a smoothing parameter. The justification is that a locally generated pressure pulse will spread quickly (velocity c) and travel a considerable fraction of a grid spacing in the finite time Δt. Further empirical testing will be needed to determine suitable values for W_p under various conditions, but it can be expected that W_p will decrease as Δt approaches its maximum. Simulation results so far have been remarkably insensitive to W_p in the range 0.2–0.8, but higher values saw the build-up of serious numerical noise, and $W_p = 0.98$ allowed total divergence of calculations.

Equation (1) is difficult in that the partial DEs are strongly coupled, and the most significant terms (under present conditions) are non-linear. The coupling problem causes no formulation difficulties for an explicit method, but both of the following techniques are directed at the non-linearities in order to improve both stability and accuracy.

2.2.3. Targeted diffusion. Firstly, consider the coefficient of U^n in the discretized version of the first part of Equation (1):

$$\begin{aligned} U^{n+1} &= U^n - \Delta t U^n \frac{\Delta U}{2\Delta x} + \cdots + \text{viscous terms} \\ &= U^n \left[1 - \frac{\Delta t}{2\Delta x} \Delta U - \Delta t\, v \left(\frac{2}{(\Delta x)^2} + \frac{2}{(\Delta y)^2} + \frac{2}{(\Delta z)^2} \right) \right] + \cdots \end{aligned} \tag{6}$$

where

$$\Delta U = (U^n_{i+1} - U^n_{i-1}).$$

The usual consideration for the coefficient (the term in square brackets) is that it must not be allowed to become negative, which could occur in e.g. diffusion-dominated problems. How-

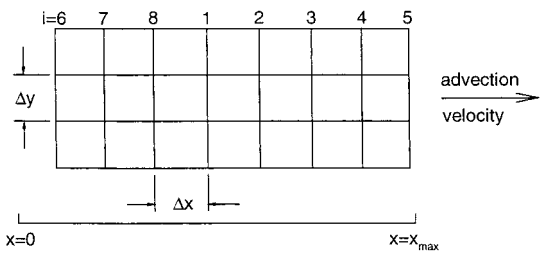

Figure 1. Typical grid position during calculations. The position of array points with index $i = 5$ is about to be redefined as $x = 0$.

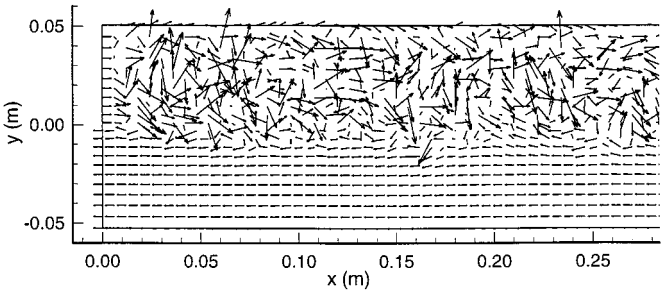

Figure 2. Effect of zero grid advection velocity. Vectors $(U - U_C, V)$ are shown in part of the plane $z = 0$ after 432 time steps of 6×10^{-5} s. Every second vector is omitted in both directions. Vectors are very similar for $x > 0.3$ m.

ever, it appears that values greater than 1.0 would be equally problematical, because numerical errors in U would be repeatedly enlarged at successive time steps. For advection-dominated flows the term in square brackets may be greater than 1.0 if ΔU is significantly negative, and therefore, if $\Delta U < 0$, U^n is replaced (in the equations but not in the stored array) by

$$U^{n'} = \left(1 + \left\{W_V \frac{\Delta t}{2\Delta x}\,\Delta U\right\}\right)U^n - \left\{W_V \frac{\Delta t}{2\Delta x}\,\Delta U\right\} \sum (\text{six neighbouring } U \text{ values})/6, \qquad (7)$$

where W_V is a constant ≥ 1. After substitution, the coefficient of U^n in Equation (6) effectively becomes

$$1 + (W_V - 1)\frac{\Delta t}{2\Delta x}\,\Delta U - W_V\left(\frac{\Delta t}{2\Delta x}\,\Delta U\right)^2 - \text{viscous terms},$$

which is always < 1.0 for negative ΔU. Ideally W_V would be equal to 1.0, and indeed that value is sufficient under some conditions, but in other cases greater values are needed to guarantee stability. The equations for V^{n+1} and W^{n+1} are similarly modified.

It can be seen from Equation (7) that the modification has an effect similar to that of viscous diffusion, and therefore its use must be justified and its effects quantified. Firstly, any local growth in numerical noise is equivalent to an injection of turbulent kinetic energy, and one way to remove excess energy is to increase viscous diffusion locally. Secondly, the troublesome values of ΔU occur mainly in the fully turbulent zones, where viscous diffusion occurs at scales far smaller than the main energy containing scales if the Reynolds number Re is high enough. Thus, temporary local increases in diffusion may have little effect on the main flow characteristics, and indeed this is implied by flow self-similarity (see later discussion) as Re increases downstream. Some tests were carried out to determine the average value of $\{W_V(\Delta t/2\Delta x)\Delta U\}$ in turbulent zones (see Equation (7)), and a typical result was -0.003, which sounds quite small considering its major beneficial effect on stability. If we assume that ΔU is negative 50% of the time, the average proportion of U^n subtracted at each time step was 0.0015, but this must be compared with < 0.001 subtracted in the viscous terms in that test. Thirdly, other tests were conducted in which 'targeted diffusion' was suddenly switched off. The result was rapid instability, even if viscosity ν was simultaneously increased by a factor of 10. Increasing ν by a factor of 100 caused relaminarization. Thus, it is clear that the present approach is targeting the stability/noise problem much more efficiently and selectively than would be the case with any global remedy. However, targeted diffusion alone is not sufficient to ensure reasonable accuracy.

2.2.4. Advected grid. The second technique for stability and accuracy is to reduce the magnitude of some of the non-linear terms. Analytically, solutions to the NS equations relative to any frame of reference moving at constant velocity will be identical except for a constant. However, if the frame of reference is fixed, the $U\,\partial U/\partial x$ terms are dominated by the large contribution to U made by local mean velocity $\bar{U}$, which tends to magnify any numerical errors in velocity gradients. Therefore, the 'advected grid' technique is employed, in which the computational grid is defined to be moving at a suitable constant advection velocity close to the mean velocity of the flow, and thus $\bar{U}$ is small relative to this grid. Several grids can be used, travelling at different velocities close to the relevant means, in cases where the mean velocity and/or the necessary resolution differ widely within the flow. However, multiple grids need to exchange information through y-direction derivatives with greater computational overheads and (possibly) reduced accuracy, so the net benefit will be flow-dependent. Testing of the two-stream mixing layer showed no advantage in using more than one grid, but the position is not yet clear for wall-bounded flows.

The computational domain itself remains fixed in space, but the grid cycles through the domain. As each grid point reaches the end of the domain, it is redefined as being at the beginning of the domain, and reset to the inlet boundary conditions. The first and last elements in the corresponding arrays are rarely at $x = 0$ and $x = x_{\max}$, and therefore they need to reference each other for the calculation of x-derivatives. A simplified representation of a grid in a typical position is shown in Figure 1. If two or more grids are used, then in general their vertical grid lines will not be aligned and some kind of interpolation scheme will be needed when calculating y-derivatives. Adjacent grids could also be given different fixed Δx spacings.

The computational effort involved in advecting a single grid is quite small. Even when all (x, z) planes were allowed to move at individual advection velocities, the additional computations added only 20% to execution times for the mixing layer simulation given below, when linear interpolation was used for exchange between grids.

An example of output from a simulation run without advecting the grid is shown in Figure 2, after 432 time steps. Initial and inlet conditions assumed no splitter plate boundary layers and used a very low level of randomness for U on the $y = 0$ grid plane only. The value of W_V was quite large at 4.0, which delayed but did not prevent computer overflow. Vectors were plotted relative to a frame moving at U_C, but the grid itself was stationary. It is clear that problems are developing first in the top half of the domain where U values, and hence non-linearity, are greatest ($U = U_H$ initially).

2.2.5. Time step. As mentioned above, the stability limit on Δt is the time taken to traverse one grid division travelling at the speed of sound, whereas the ideal time step would be related to the characteristic time of the fine scales of turbulent motion (which is still rather brief in most cases). The determination of Reynolds number does not involve any reference to pressure or to speed of sound, so it should be possible to change from a typical fluid (say, air) to another fluid of the same kinematic viscosity but lower sonic speed, without affecting the flow. A larger time step is then available for the new (possibly hypothetical) fluid. However, an 'incompressible' flow must not be allowed to become compressible in the conventional sense by having a sonic speed too low. By contrast, the assumption of true incompressibility makes sonic speed infinitely fast, a more extreme case, and therefore the effects of physical pressure fluctuations must be resolved in some sense throughout the entire computational domain at each time step.

3. EXAMPLE: TWO-STREAM MIXING LAYER

The following results are presented as a first indication of the AGE method's potential for producing useful information from modest computational resources; they are not meant to be a definitive example of its application. Most likely the method itself will be developed further in the light of experience with simulations of other turbulent flows. Much of the testing so far has involved multiple advected grids and inlet conditions (without splitter plate boundary layers) that are not directly relevant to the present example.

Another aspect to mention is that experimental results for mixing layers vary quite widely, as noted by Rogers and Moser [11]. However, only two experiments will be considered here, both with velocity ratio U_L/U_H of about 0.6, chosen for the following reasons. Firstly, the

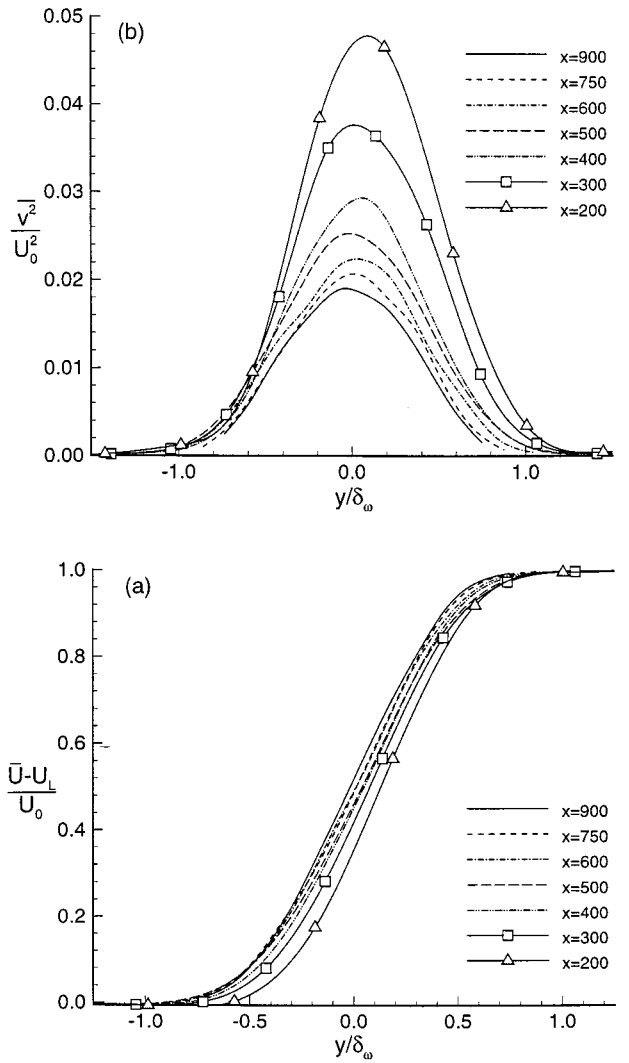

Figure 3. Approach to self-similarity. Profiles of (a) mean velocity, and (b) variance of transverse velocity fluctuations, for seven streamwise stations.

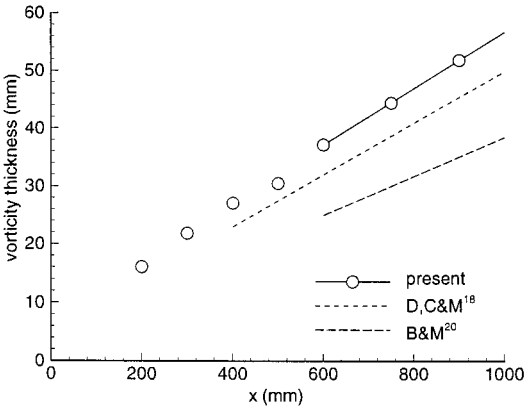

Figure 4. Streamwise development of vorticity thickness for the present simulation and for the self-similar regions of experiments [18,20].

present author was already familiar with data from the mixing layer described by Delville *et al.* [18] (see Reference [19]). The Reynolds number there is about 1.5 times higher than reached by the simulation. Secondly, the experiment of Bell and Mehta [20] considers two types of inlet condition in detail, overlaps with the present work in terms of Reynolds number, and was used for comparison purposes by Rogers and Moser [11]. Present results will also be compared with the pseudospectral simulation of a temporally growing mixing layer from the last mentioned authors that reached about half the present maximum *Re*.

3.1. Flow description

Two parallel streams of fluid travelling in the same direction at different uniform velocities are kept apart by a thin splitter plate (which is horizontal in the present work, with the high-speed stream above it). At the end of the plate the streams begin to interact and form a planar mixing layer. The nature of the initial interaction depends strongly on the type and thickness of the boundary layers on the splitter plate (e.g. Reference [20]), but further downstream the mixing layer becomes self-similar (or self-preserving), i.e. profiles of mean velocity and Reynolds stresses are unchanging when normalized with appropriate length and velocity scales [21]. The latter scale is generally U_0, the difference between U_H and U_L, the high- and low-speed stream velocities relative to the splitter plate. Another important velocity is the (assumed) convection velocity $U_C = (U_H + U_L)/2$.

There are at least four measures of length scale in common use, namely, visual thickness, vorticity thickness, momentum thickness, and Gaussian error function parameter. Visual thickness is hard to determine precisely, but it is usually about twice the value of vorticity thickness. The latter is defined by

$$\delta_\omega = \frac{U_0}{(\partial \bar{U}/\partial y)_{\max}}.$$

Vorticity thickness is used as the length scale by Delville *et al.* [18] and is also used in this paper. Momentum thickness is used by Moser and Rogers [12] and Rogers and Moser [11], while Bell and Mehta [20] use the value of δ that gives the best fit to the error function velocity profile suggested by Townsend [21]. Moser and Rogers [12] also utilize the error function profile for initializing their temporal simulations. Rogers and Moser [11] state that the ratios

between δ_ω and momentum thickness for their results and for an error function profile are 4.8 and 4.44 respectively, and for the Bell and Mehta [20] results $\delta_\omega = \delta\sqrt{\pi}$ will be used.

3.2. Domain and boundary conditions

The computational domain extends downstream from the trailing edge of the splitter plate, and ideally is long enough for the mixing layer to reach self-similarity. The height must be sufficient for unfettered free stream conditions to exist for the full length. Periodic boundary conditions are used in the z-direction, and therefore the width must be at least twice the distance at which correlations in the z-direction die out. In spite of the extra width requirement, periodic boundary conditions are easy to implement and do not generate spurious input to the mixing layer near the inlet where it is very receptive to small disturbances. Far enough above and below the layer, the boundary conditions are $U = U_H$ or U_L, $V = W = 0$, and $P =$ constant; the possibility that $\bar{V} \neq 0$ at the edge because of entrainment is neglected. These conditions are implemented in the form of damping layers at the $\pm y$ edges of the main computation zone (details below).

Inflow boundary conditions are $U = U_H$ or U_L except at y values near the centreplane where splitter plate boundary layers are crudely modelled; also $V = W = 0$, and $P =$ constant. Outflow from the main computation zone goes into a long damping zone, at the end of which $V = W = 0$, $P =$ constant and $U = U_C$. Better conditions at the outlet might be $U = \bar{U}(y)$, or possibly $\partial U/\partial x = 0$, but the present condition seems to work within a reasonably long damping zone and does not require prior knowledge or concurrent calculation of $\bar{U}(y)$. Temporal simulations [11] can use periodic outflow–inflow boundaries as well as spanwise periodicity, a simplification not available in spatial simulations.

The procedure for damping near boundaries is that values of variables are modified slightly at every time step so as to reduce the difference between their current values and the relevant boundary conditions, the aim being to prevent reflections by 'absorbing' fluctuations. The degree of modification is progressively greater nearing the boundary (e.g. for the outlet damping zone the difference was reduced by 1%, 2%, 3%,… per time step at successive grid points). The one exception is U in the outlet damping zone: the mismatch between $\bar{U}(y)$ leaving the main calculation zone and U_C at the boundary causes unwanted pressure deviations, and results are better if U remains undamped approaching the outlet. Boundary conditions for simulations in which acoustic behaviour is an important result can be far more sophisticated, e.g. References [22,23].

Details of the example calculations are as follows: $U_H = 16.0$ m s^{-1}, $U_L = 9.6$ m s^{-1} (thus $U_0 = 6.4$ m s^{-1} and $U_C = 12.8$ m s^{-1}); there were $400 \times 81 \times 121$ grid points in x, y and z, of which the upper and lower damping layers occupied 20 points each (in y) and the outlet damping zone occupied 40 points (in x); $\Delta x = 3$ mm, $\Delta y = 2$ mm at the centreplane and 2×1.02, 2×1.02^2, 2×1.02^3,… mm, above and below the centreplane ($y = 0$); $\Delta z = 3$ mm at the $z = 0$ midplane and 3×1.01, 3×1.01^2, 3×1.01^3,… mm either side of it. Thus, the total domain size was $1.2 \times 0.242 \times 0.48$ m, and the undamped domain was $1.08 \times 0.097 \times 0.48$ m. About 54% of all grid points were involved in boundary damping, but it has been found recently that the upper and lower damping layers were thicker than necessary.

A single advected grid was used with advection velocity equal to U_C. The working fluid was given the characteristics of atmospheric air except that its nominal pressure was reduced to yield a sonic velocity c of 25 m s^{-1} (density was unchanged). The nominal Mach number is $U_0/c = 0.26$, inside the accepted limit of 0.3 for 'incompressible' flow. The time step was set at 6×10^{-5} s, i.e. 3/4 of the maximum allowable. The pressure smoothing and targeted diffusion

parameters were $W_p = 0.2$ and $W_V = 2.7$ for the main results. As indicated previously, results were affected very little by changes to W_p in the range 0.2–0.8; the situation is not so clear-cut for W_V, but changes in the range 2.5–3.6 had limited effect.

The splitter plate boundary layer on the high-speed side was emulated (except where otherwise noted) by reducing the inlet U in the innermost high-speed grid plane to $0.5U_H \pm R$, where R is a random number of average magnitude $0.1U_H$, and R is recalculated at every second time step and for every grid point in z. In the adjacent high-speed grid plane the values were $0.9U_H$ and $0.07U_H$, respectively. An analogous boundary layer was emulated on the low-speed side. These emulations are somewhat thinner than the real boundary layers in the experiments, but undoubtedly have greater momentum defects. The hope was that the flow would become self-similar relatively quickly, noting Bell and Mehta's [20] results for turbulent and laminar inlet conditions.

3.3. Output

Three types of output were obtained from the simulations. Firstly, rakes of 12 'probes' spaced 6 mm apart in y were inserted at three spanwise (30 mm spacing) and three streamwise positions, in order to record continuous time-series of U, V, W and P. Each run included probes at $x = 900$ mm and at two upstream stations, sampling at 8333 Hz (i.e. every second time step) with linear interpolation between adjacent grid points in x (allowing for grid advection). The resulting data files were processed using software normally applied to hot wire data from experiments. Data from corresponding spanwise positions were processed together. Secondly, 2D snapshots of the flow in the (x, y) and (x, z) centreplanes were taken occasionally, from which contour, vector and sectional streamline plots were prepared. Finally, 3D chunks of data were extracted as needed, primarily (in this paper) for plots of pressure surfaces.

3.4. Computation times

Travelling at U_C, a particle of fluid requires 1406 time steps to pass through the main calculation zone, and therefore to avoid start-up transients data from the first 2048 time steps were omitted from the analysis. At $x = 900$ mm, data from a total of 12 288 time steps (0.74 s) were analysed but only 1/3 as much at other streamwise stations. The 0.74 s run took slightly less than 30 h of CPU time on a DEC Alpha 4/200 computer. It was coded in VMS Fortran (single precision) and occupied about 125 Mbyte of memory. Note that computation time is directly proportional to the number of grid points unless array size exceeds computer memory, in which case page faulting of virtual memory can become a significant overhead. At $x = 900$ mm the Reynolds number $Re = U_0\delta_\omega/\nu$ is 22 200 (nominally), about double the 10 800 reached by Rogers and Moser [11]. It is hard to compare computing effort between simulations that are not exactly equivalent, and in any case Rogers and Moser [11] do not give figures. However, they used about four times as many spectral modes as Moser and Rogers [12], and in that case up to 380 h on a Cray Y-MP were needed for mixing layer simulations of related type.

An advantage of temporal simulations is that flow statistics can be obtained from spatial averages across complete (x, z) planes allowing shorter simulation runs. The present simulation could be set up as a temporal simulation, given appropriate initial and boundary conditions (including $U_C = 0$), in which case computational effort would be similar to that for the start-up transient presently discarded.

4. RESULTS AND DISCUSSION

Mean velocity profiles $(\bar{U} - U_L)/U_0$ as a function of y/δ_ω, at seven streamwise stations are presented in Figure 3(a). The slow drift towards the low-speed side is at least qualitatively correct [11], and profile shapes are reasonably close after the first few stations. However, adequate collapse of mean velocity to a single profile is not a strong indicator of self-similarity, whereas Reynolds stress profiles are more sensitive. Of the Reynolds stress profiles for the present results, $\overline{v^2}$ shows the greatest streamwise variation. Profiles of $\overline{v^2}/U_2^0$ are plotted in Figure 3(b), where it can be seen that the flow is approaching self-similarity but probably has not quite reached that state.

Streamwise growth of vorticity thickness is plotted in Figure 4. The solid line is the best fit to the last three points, and the other lines represent self-similar growth from the experiments. The effect of strong splitter plate boundary layers is apparent in a fairly large δ_ω value at $x = 0$, and the apparent origin x_0 of the simulated layer is well upstream at $x_0 \approx -150$ mm. The normalized slope of the line is $(\mathrm{d}\delta_\omega/\mathrm{d}x)U_C/U_0 = 0.096$, near the top of the typical range (0.081–0.098) quoted by Rogers and Moser [11]. For Delville *et al.* [18] the slope is in the middle of the typical range, and for Bell and Mehta [20] the slope of 0.067 is a little below it.

The linear growth of transverse length scale should be accompanied by a similar growth of longitudinal scale of dominant structures, which can be inferred from peak frequencies in power spectra. Usually, v-spectra show the most definite peaks; v-spectra for several stations relative to the virtual origin are presented in Figure 5. The inlet 'boundary layers' affect the $x - x_0 = 200$ mm curve, but a good peak around 400 Hz is apparent at 250 mm. At 500 mm the peak would be around 200 Hz, and at 1050 mm the peak is halved again to about 100 Hz, as expected (δ_ω grows by a factor of about 4 over the same range). This implies that on

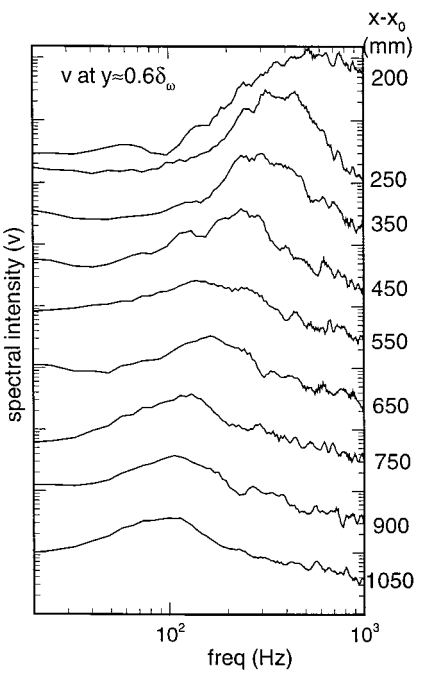

Figure 5. Streamwise development of the power spectrum of transverse velocity fluctuations (y-axis shifted).

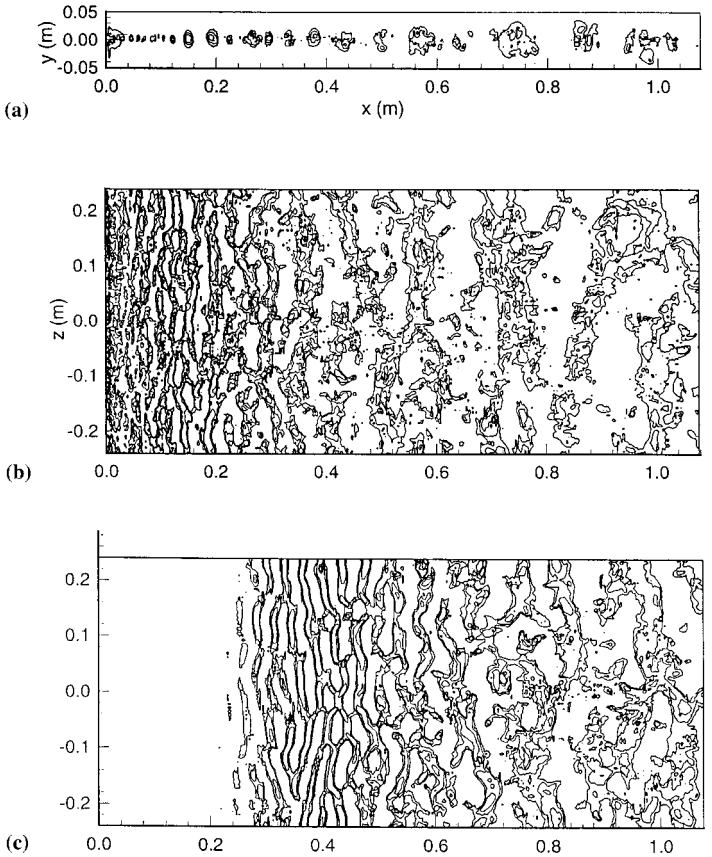

Figure 6. Contours of instantaneous pressure fluctuations; contour levels -2.0, -4.0, -8.0 Pa. (a) Fluctuations in the plane $z = 0$, and (b) in the plane $y = 0$ at the same instant; (c) fluctuations at $y = 0$ for a run with no splitter plate boundary layers.

average four dominant structures have merged into one over the given range, though not necessarily by a formal pairing process.

Fluid pressure in the core of a vortex-like rotational structure must be relatively low, as discussed earlier. Contours indicating low pressure areas in the planes $z = 0$ and $y = 0$ are shown for a certain time instant in Figure 6(a,b), and they do give an impression of structure development within the flow. In the spanwise view (Figure 6(b)) it can be seen that the initial

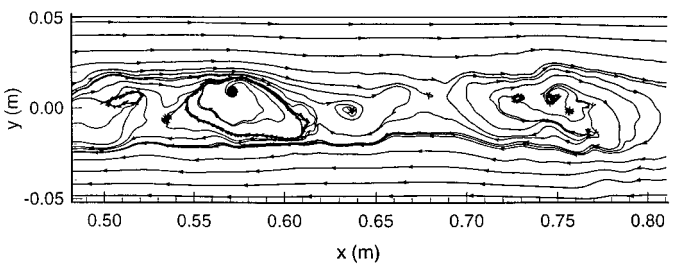

Figure 7. Sectional streamlines calculated from part of the velocity field corresponding to Figure 6(a).

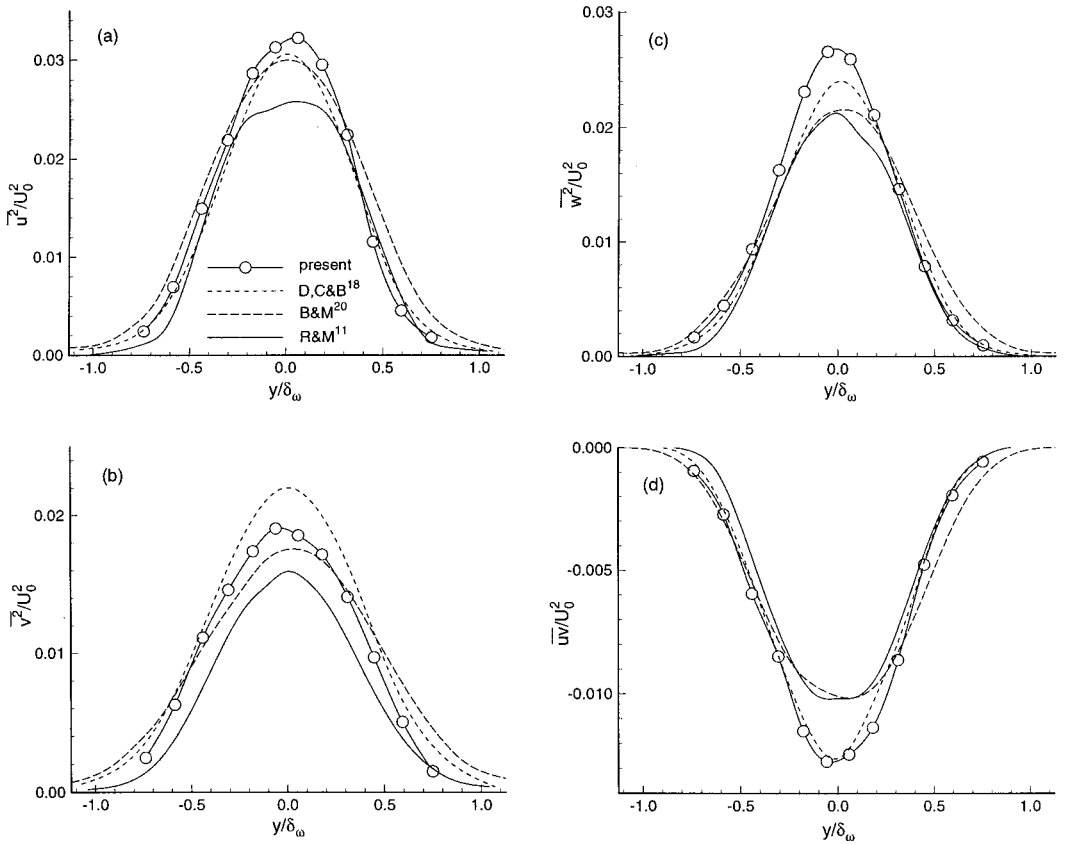

Figure 8. Profiles of Reynolds normal and shear stresses in self-similar regions from experiments (Delville *et al.* [18] and Bell and Mehta [20]) and simulations (Rogers and Moser [11], and the present work at $x = 900$ mm).

structures are mainly quite extended in the spanwise direction (although they are always at least somewhat 3D), and they appear very early in the domain. Further downstream the structures appear to be more turbulent and 3D, and their scale is much larger, as expected from the v-spectra (Figure 5). For comparison, low pressure contours from a run with no inlet boundary layers, and a very low level of U randomization at $y = 0$ only, are shown in Figure 6(c). No 'forcing' at particular frequencies, as often used in numerical simulations (e.g. References [12,14,15]), has been applied in any of the present work. Now the initial structures have a more laminar character than in Figure 6(b), but they are still 3D with a characteristic branching and joining at various places. The description [24] 'helical pairing' fits the initial branching and joining behaviour quite well. Further downstream the structures become turbulent but they are not as developed as in the main simulation.

Figure 7 shows sectional streamlines calculated for part of the plane from Figure 6(a). They are highly reminiscent of streamlines plotted from X-wire data—see Reference [19] for an example. In both cases the streamlines often spiral outwards from the cores of well-developed structures, the one at $x = 0.75$ m in Figure 7 being typical. Bisset *et al.* [25] demonstrated in both experimental data and a kinematic model of a planar far-wake that outward spiralling correlates closely with transverse momentum transfer (i.e. substantial $\overline{uv}$, the Reynolds shear stress).

Reynolds normal and shear stresses at $x = 900$ mm are compared with experimental and spectral simulation results in Figure 8. All flows begin from splitter plates with turbulent boundary layers. The range of Reynolds numbers is about 3:1 but is not likely to have a significant bearing on the comparison, as all flows are either self-similar or not far from it. The Bell and Mehta [20] results were given again in Figure 4 of Reference [11] with better resolution, therefore this was used as the source. For both those papers the results shown here are averages over several δ_ω values in the self-similar region, and they have been converted to a y/δ_ω abscissa using the length scale relationships mentioned previously. The present simulation profiles have not been corrected for drift towards the low-speed side.

There is substantial disagreement between the two experiments in all profiles except $\overline{u^2}$ (Figure 8(a)) about peak (centreplane) values, although the general shapes of the profiles are similar. For Reynolds shear stress $\overline{uv}$, which represents transverse momentum transfer, the difference is consistent with different growth rates of vorticity thickness (Figure 4) for the two experiments. (Although, as Townsend [21] (pp. 196) points out, δ_ω at any point is the integrated result of all upstream momentum transfer, and the approach to self-similarity may be gradual). Clearly the disagreements between the two simulations, and between simulations and experiments, are of the same order.

The general tendency for the spectral simulation profiles [11] to be weaker may be related to the temporal nature of that simulation: the velocity ratio U_H/U_L is effectively 1.0 instead of 0.6 as used in the experiments and the present spatial simulation. The manner of growth might change in subtle ways when there is no difference at all between upstream and downstream influences. Experiments with lower velocity ratios have not (to the author's knowledge) shown large effects on normalized Reynolds stress profiles, but velocity ratios approaching 1.0 are difficult experimentally. Profiles from the present simulation tend to be a little stronger than the others (except for $\overline{v^2}$, Figure 8(b)), but this could be a product of both imperfect self-similarity and non-ideal settings of the simulation parameters.

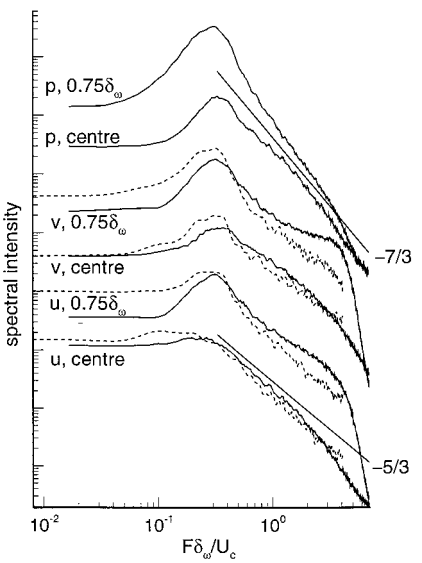

Figure 9. Power spectra of velocity components from (- - -) experiment [26] and (—) simulation at two y positions, and power spectra of pressure fluctuations. Curves are offset vertically.

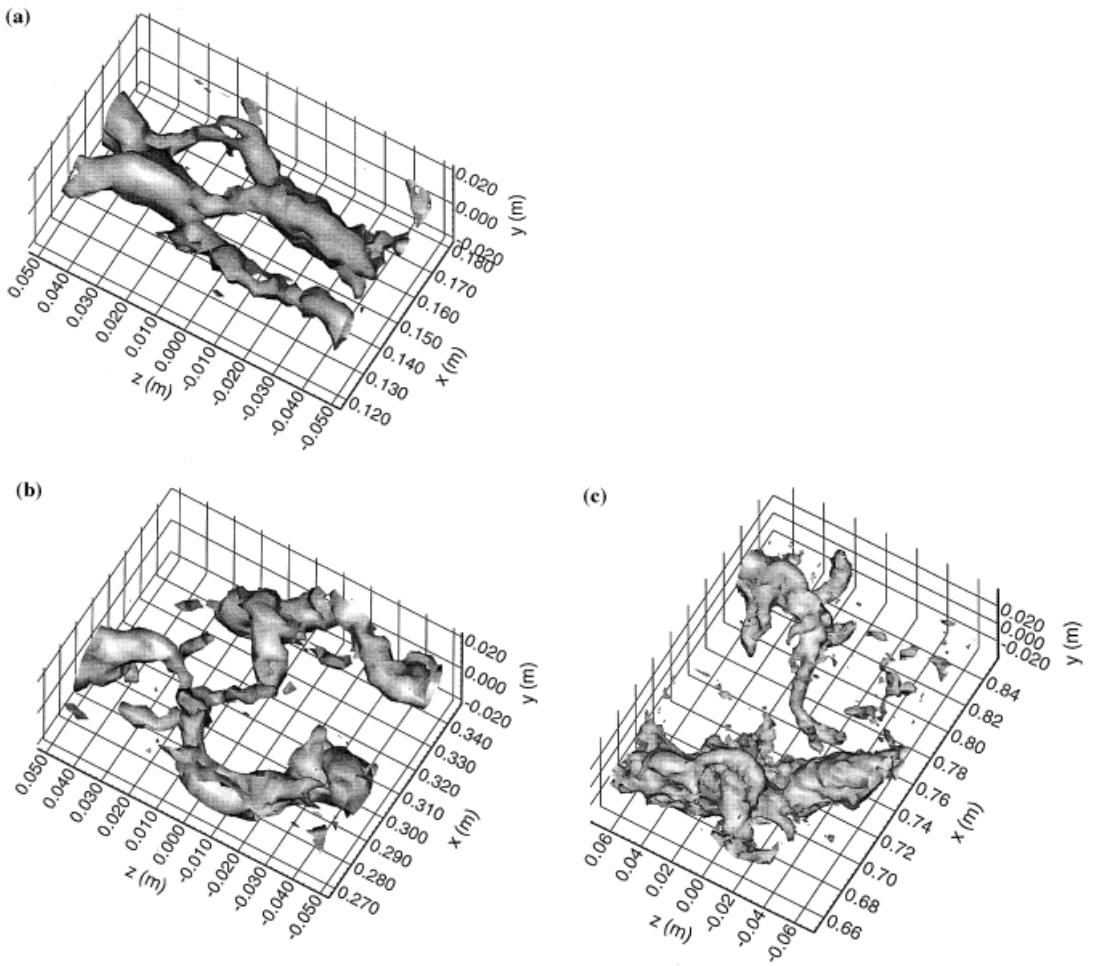

Figure 10. Vortex-like structures in the same patch of fluid at three different times. The relative pressure surface $p = -4.0$ Pa is shown for (a) and (b), and $p = -3.0$ Pa for (c). Note that the field of view becomes larger for successive parts of the figure.

One of the most difficult tasks for a numerical simulation is to achieve correct spectral distributions of turbulent fluctuations. Figure 9 shows power spectra for u, v and p (normalized by their respective variances) at $x = 900$ mm and at two y positions, as functions of normalized frequency $F\delta_\omega/U_C$ (a form of Strouhal number). The comparison experimental results for u and v were generated from data from the mixing layer of Reference [19] which were supplied to an ERCOFTAC workshop [26]. Peak values in the spectra show minor discrepancies that could be related to the presence of energy at rather low frequencies in the experiment, not captured by the simulation. Near the centreplane, the energy cascade towards higher frequencies in the simulation follows the experiment moderately well, and the u spectrum shows more than half a decade of inertial range followed by gradual roll-off. At $y = 0.75\delta_\omega$ there are departures for u and especially v, with excess energy at frequencies around ten times the peak frequency and then a rather sharp roll-off. The reason for this behaviour is still being investigated, but in any case the total energy in the problem spectra is more than an order of

magnitude (Figure 8) below that in spectra from near the centreplane. The spectrum of pressure fluctuations near the centreplane is marginally shallower than the $-7/3$ slope expected in the inertial range, whereas the pressure spectrum at $y = 0.75\delta_\omega$ is somewhat steeper. Overall, the spectral results are not ideal, but in conjunction with the Reynolds stress distributions (Figure 8) they support the claim that the AGE method can produce fairly realistic results at fully turbulent Reynolds numbers.

An important factor for quality of simulation results is resolution with respect to both time and space. Time advancement here is not a significant source of error. Results from trials with $\Delta t = 4 \times 10^{-5}$ and 8×10^{-5} s were virtually indistinguishable from those shown with $\Delta t = 6 \times 10^{-5}$ s, indicating that higher-order time advancement schemes would not be beneficial. Spatial resolution is not as easily tested. Ideally grid refinement would be carried out, but first a larger domain is needed to ensure that the flow really is self-preserving, and then the already larger number of grid points increases as the cube of the rate of grid refinement, and the time step stability limit decreases. The computer resources needed to achieve statistically well-converged results in such a case were not available to the author. However, it is possible to estimate turbulence length scales and compare them with the grid. Using u data from the centreplane and the usual assumption of isotropy, the Taylor microscale and Kolmogorov viscous scale were estimated to be about 7 and 0.15 mm respectively, at $x = 900$ mm. Thus the grid resolution (≥ 2 mm) for inertial scales may be adequate, but viscous scales are not fully resolved. Lesieur and Métais [1] suggest that an underresolved DNS of a flow (a 'pseudo-direct simulation') could be considered to be a kind of implied LES in the sense that the too-coarse grid has the same dissipative effect as an LES subgrid model. Presumably the quality of result will improve as scale truncation decreases, yet a small degree of truncation in the viscous range greatly reduces computing requirements (the inverse of the grid refinement problem noted above).

A strength of any direct numerical simulation is its ability to give a 'physical' picture of the development of flow structure, e.g. the full-colour numerical snapshots (including pressure surfaces) in Reference [15]. For the present work, 16 sequential views of low-pressure surfaces were obtained from a patch of fluid as it travelled the length of the computational domain. Only three of the views will be presented, partly due to the scope of this paper and partly because a planned video will show the whole structure development process much more clearly. The results can be related to Figure 6(a,b), but that figure shows different stages of development for different areas of fluid at a single time instant, as opposed to development in the same patch of fluid at a series of different times.

Pressure isosurfaces ($p = -4.0$ Pa) for a small patch of fluid not far from the inlet are shown in Figure 10(a). The viewing direction is obliquely downstream from the high-speed side, and the apparently left-handed set of axes is accidental. The low-pressure regions seem quite well-defined, and there seems to be a lot of 'helical pairing' [24] underway at this stage.

The patch of fluid has travelled further downstream in Figure 10(b), and the apparently strong structure at the right rear of the previous figure has broken apart, leaving a V-shaped section in the middle. Quite soon afterwards, the V-shaped part also vanishes. It is apparent that the main structures are already larger and more complex (turbulent) than they were near the inlet, but there has been no formal, highly deterministic pairing of structures.

By the time of Figure 10(c), much further downstream, the low-pressure regions are much larger and more convoluted (note the larger field of view). The rearward structure is beginning to fall apart, and a piece of it is being stretched down towards the forward structure with an almost streamwise orientation. In the final views of the sequence (not shown) the stretched piece becomes longer and thinner, and eventually vanishes.

It is interesting that smaller structures partly retain their identities for a while after merging to form larger ones. Pressure surfaces for the latter are consequently very convoluted, and possibly the large structures are less stable than they would be if they had a more regular make-up. Velocity and vorticity fields associated with structures would be interesting also, but these are omitted because of lack of space. For example, (V, W) vectors in (y, z) planes cutting through the thin streamwise structure of Figure 10(c) show, as expected, strong rotational motion around the low pressure core, and streamlines spiral inwards as it is stretched.

5. CONCLUSIONS

The advected grid explicit (AGE) method for numerical simulation of 'incompressible' turbulent shear flows has been presented, and has the following features:

- The NS equations are used for momentum, and mass continuity and an equation of state link pressure with density (not assumed identically constant), in a velocity–pressure formulation.
- Time advancement is entirely explicit.
- Spatial representation is localized (e.g. finite difference) and centred; viscous scales were not fully resolved in the test flow without ill effects (a kind of implied LES).
- The pressure field is locally smoothed between time steps.
- Numerical instabilities are efficiently reduced by targeted diffusion.
- Magnitudes of non-linear terms are reduced on the advected grid(s).
- Time step limitations are managed to an extent by controlling sonic speed in the fluid.
- Computation time scales directly on the number of grid points (virtual memory issues aside), and is relatively short for a DNS method.

None of the above features are claimed to be a totally new concept (and some are common practice in other contexts), but it is the unique combination of features that constitutes the AGE method.

The example simulation of a canonical free shear flow, namely the two-stream mixing layer, was quite successful in many respects (including computational speed), even though the method has not been optimized. The AGE method should also be applicable for simulation of subsonic compressibility effects, and for simulation of wall-bounded turbulent shear flows. Further developments of the method can be expected as it is applied to new flows.

ACKNOWLEDGMENTS

Thanks to Prof J.P. Bonnet of Poitiers University for permission to use data from CEAT experiments [26] in Figure 9. Thanks also to A/Prof D.H. Wood (Newcastle) for use of software to prepare figures. The author was an ARC funded research associate with Prof R.A. Antonia (Newcastle) during early stages of this work.

REFERENCES

1. M. Lesieur and O. Métais, 'New trends in large-eddy simulations of turbulence', *Ann. Rev. Fluid Mech.*, **28**, 45–82 (1996).
2. P.J. Roach, *Computational Fluid Dynamics*, 2nd ed, Hermosa, Albuquerque 1976.
3. R. Peyret and T.D. Taylor, *Computational Methods for Fluid Flow*, Springer, New York, 1983.
4. C.A.J. Fletcher, *Computational Techniques for Fluid Dynamics*, Vols I and II, Springer, Berlin, 1991.

5. J.H. Ferziger and M. Peric, *Computational Methods for Fluid Dynamics*, Springer, Berlin, 1996.
6. P.R. Spalart, R.D. Moser and M.M. Rogers, 'Spectral methods for the Navier–Stokes equations with one infinite and two periodic directions', *J. Comput. Phys.*, **96**, 297–324 (1991).
7. P. Moin and J. Kim, 'The structure of the vorticity field in turbulent channel flow. Part 1. Analysis of instantaneous fields and statistical correlations', *J . Fluid Mech.*, **155**, 441–464 (1985).
8. J. Kim and P. Moin, 'The structure of the vorticity field in turbulent channel flow. Part 2. Study of ensemble-averaged fields', *J. Fluid. Mech.*, **162**, 339–363 (1986).
9. J. Kim, P. Moin and R.D. Moser, 'Turbulence statistics in fully developed channel flow at low Reynolds number', *J. Fluid Mech.*, **177,** l33–166 (1987).
10. P.R. Spalart, 'Direct simulation of a turbulent boundary layer up to $R_\theta = 1410$', *J. Fluid Mech.*, **187**, 61–98 (1988).
11. M.M. Rogers and R.D. Moser, 'Direct simulation of a self-similar turbulent mixing layer', *Phys. Fluids*, **6**, 903–923 (1994).
12. R.D. Moser and M.M. Rogers, 'The three-dimensional evolution of a plane mixing layer: pairing and transition to turbulence', *J. Fluid Mech.*, **247**, 275–320 (1993).
13. M.M. Rai and P. Moin, 'Direct simulation of turbulent flow using finite difference schemes', *J. Comput. Phys.*, **96**, 15–53 (1991).
14. R.W. Metcalfe, S.A. Orszag, M.E. Brachet, S. Menon and J.J. Riley, 'Secondary instability of a temporally growing mixing layer', J. Fluid Mech., **184**, 207–243 (1987).
15. P. Comte, M. Lesieur and E. Lamballais, 'Large- and small-scale stirring of vorticity and a passive scalar in a 3-D temporal mixing layer', *Phys. Fluids A*, **4**, 2761–2778 (1992).
16. A.J. Chorin, 'A numerical method for solving viscous flow problems', *J. Comput. Phys.*, **2**, 12–26 (1967).
17. C.W. Hirt and F.H. Harlow, 'A general corrective procedure for the numerical solution of initial-value problems', *J. Comput. Phys.*, **2**, 114–119 (1967).
18. J. Delville, Z. Chahine and J.P. Bonnet, 'Experimental study of an incompressible, plane mixing layer by temporal and spectral analysis', in G. Comte-Bellot and J. Mathieu (eds.), *Advances in Turbulence*, Springer, Berlin, 1987, pp. 435–444.
19. J.P. Bonnet, J. Delville and M.N. Glauser, 'Workshop on eddy structure identification in free turbulent shear flows', *ERCOFTAC Bulletin*, **17**, 41–51 (1993).
20. J.H. Bell and R.D. Mehta, 'Development of a two-stream mixing layer from tripped and untripped boundary layers', *AIAA J.*, **28**, 2034–2042 (1990).
21. A.A. Townsend, *The Structure of Turbulent Shear Flow*, Cambridge University Press, Cambridge, 1976.
22. T. Colonius, S.K. Lele and P. Moin, 'Boundary conditions for direct computation of aerodynamic sound generation', *AIAA J.*, **31**, 1574–1582 (1993).
23. M.E. Hayder and E. Turkel, 'Nonreflecting boundary conditions for jet flow computations', *AIAA J.*, **33**, 2264–2270 (1995).
24. C. Chandrsuda, R.D. Mehta, A.D. Weir and P. Bradshaw, 'Effect of free-stream turbulence on large structure in turbulent mixing layers', *J. Fluid Mech.*, **85**, 693–704 (1978).
25. D.K. Bisset, R.A. Antonia and L.W.B. Browne, 'Spatial organization of large structures in the turbulent far wake of a cylinder', *J. Fluid Mech.*, **218**, 439–461 (1990).
26. CEAT, Data supplied by the Centre d'Etudes Aérodynamics et Thermiques at Poitiers University, France, to the ERCOFTAC Workshop on Structure Identification in Free Turbulent Shear Flows, Poitiers, France, 15–16 October, 1992.

